Journal of Water Process Engineering 66 (2024) 106038

Contents lists available at ScienceDirect

Journal of Water Process Engineering

journal homepage: www.elsevier.com/locate/jwpe

Boosting adsorption of ciprofloxacin on Fe_3O_4 nanoparticles modified sepiolite composite synthesized via a vacuum-filtration assisted coprecipitation strategy

Shiyuan Kang [a,b], Bing Yi [a], Xin Nie [b,**], Quan Wan [a,b,c,*], Hai Yang [a,**]

[a] Hunan Provincial Key Laboratory of Environmental Catalysis and Waste Recycling, College of Materials and Chemical Engineering, Hunan Institute of Engineering, Xiangtan 411104, China
[b] State Key Laboratory of Ore Deposit Geochemistry, Research Center of Ecological Environment and Resource Utilization, Institute of Geochemistry, Chinese Academy of Sciences, Guiyang 550081, China
[c] CAS Center for Excellence in Comparative Planetology, Hefei 230026, China

ARTICLE INFO

Editor: Laura Bulgariu

Keywords:
Fe_3O_4 nanoparticles modified sepiolite composite
Vacuum-filtration assisted coprecipitation
Ciprofloxacin
Adsorption mechanism

ABSTRACT

Treatment of antibiotics-containing wastewater is imperative for ensuring environmental and public health. However, effectively removing antibiotics in environment is still a great challenge. Fabrication of sepiolite-supported iron oxide nanomaterials with large specific surface area and high reactivity is a promising solution for efficient antibiotics removal. In this work, a highly dispersed Fe_3O_4 nanoparticle modified sepiolite composite (Fe_3O_4-sep-vacuum) was synthesized in-situ by employing a novel vacuum-filtration assisted coprecipitation strategy for the first time. Fe_3O_4-sep-vacuum exhibited the highest adsorption capacity to ciprofloxacin compared with those of pure Fe_3O_4 nanoparticles, sepiolite, and those composites obtained by traditional coprecipitation methods. Approximately 93 % of CIP (20 mg/L) could be removed by Fe_3O_4-sep-vacuum within 20 min at initial pH 6.0. The kinetic and adsorption isotherms followed pseudo-second-order and Temkin models, respectively. The maximum adsorption capacity (q_m) of Fe_3O_4-sep-vacuum for CIP was 18.4 mg/g at initial pH 6.0. The solution pH, temperature, coexisting divalent cations, and HA concentration were demonstrated to play substantial roles in the adsorption processes of ciprofloxacin on Fe_3O_4-sep-vacuum surface. The Fe_3O_4-sep-vacuum maintained excellent stability and reusability during CIP adsorption process. Electrostatic interactions play a decisive role in the adsorption process of ciprofloxacin by Fe_3O_4-sep-vacuum. Hydrogen bonds and hydroxyl groups on the Fe_3O_4-sep-vacuum surface also play important roles in the adsorption process of ciprofloxacin. Fe_3O_4-sep-vacuum also exhibited excellent adsorption capacity to ofloxacin. These results indicate that the vacuum-filtration assisted coprecipitation strategy could be used to fabricate monodispersed nanoparticles modified sepiolite composites, which could be acted as promising materials for highly efficient remediating antibiotics contaminated wastewater.

1. Introduction

Antibiotics are widely used to treat bacterial infections in humans and animals. However, a large amount of antibiotics-containing wastewater are directly or indirectly released continuously into aquatic environments through improper disposal of expired or unused medication, veterinary, livestock, excreta of animals and human containing non-metabolized forms after intake, and unintentional discharges of municipal and industrial wastewaters from hospitals and pharmaceutical manufacturers [1–3]. Various antibiotics have been frequently detected in different geographical regions worldwide in concentrations ranging from ng/L to mg/L in various aquatic environments, including domestic wastewater, hospital wastewater, pharmaceutical industries effluent, livestock effluent, surface water, groundwater, and drinking water [4,5]. Antibiotics could accumulate persistently in all the aquatic environments, resulting in adverse effects on the environment and

* Correspondence to: Q. Wan, State Key Laboratory of Ore Deposit Geochemistry, Research Center of Ecological Environment and Resource Utilization, Institute of Geochemistry, Chinese Academy of Sciences, Guiyang 550081, China.
** Corresponding authors.
E-mail addresses: niexin2004@163.com (X. Nie), wanquan@vip.gyig.ac.cn (Q. Wan), yanghai1001@163.com (H. Yang).

https://doi.org/10.1016/j.jwpe.2024.106038
Received 2 July 2024; Received in revised form 20 August 2024; Accepted 20 August 2024

human health even at trace level of concentration, creating antibiotic-resistant bacteria and antibiotic-resistance genes, thereby posing a potential threat to aquatic ecosystem and human health [6–9]. In recent years, considerable concern has been made to control the prudent use of antibiotics in various countries, which highlights the necessity for stricter enforcement of regulatory measures and policies as well as effective removal methods. Therefore, effective removal of antibiotics from the aquatic environment is imperative for ensuring environmental and public health.

Various wastewater treatment techniques, including chemical oxidation, catalytic degradation, biological treatment process, membrane filtration, adsorption, and advanced oxidation technologies, have been developed to remove antibiotics from aquatic environments [2,10–12]. As a high effective, facile operation, and cost saving technology, adsorption is the most widely used and the most competitive wastewater treatment technology for the elimination of antibiotic pollutants in the aquatic environment. Various adsorbents, such as biochar, activated carbon, porous carbon, carbon nanotubes, polymers, metal–organic frameworks, zeolite, metal and metal oxide nanomaterials as well as their composites, and natural mineral materials, have been used for removing antibiotics from water [13–18]. Among them, iron oxide nanomaterials have been shown to be effective adsorbents due to their high specific surface areas, low cost, high biosecurity, and large adsorption capacities [15,19]. Nonetheless, iron oxide nanomaterials synthesized by conventional methods (e.g., coprecipitation, sol-gel combustion or solid-phase synthesis), are extremely unstable to susceptibility aggregate into large particles, resulting in lowered number of adsorption sites and adsorption capacities [20]. In this regard, synthesis of highly monodispersed and stable iron oxide nanomaterials by dispersing them onto support materials may be a good choice to address above problems.

As a one-dimensional (1D) hydrous magnesium-rich silicate clay mineral, sepiolite (sep) is regarded as a hopeful natural nanomaterial for effectively purifying environmental pollutants due to its unique nanoporous structure, large specific surface area, affluent surface-active groups, and better ion-exchange capacity [21,22]. The presence of abundant nanoporous structural cavities of tunnels and channels in a cross-section of sepiolite allows small molecules to be stably immobilized inside them [23]. The abundant highly active silanol groups (Si-OH) on the surface of sepiolite are also beneficial for selective adsorption of diverse organic molecules, inorganic ions, and even nanoparticles, making sepiolite could be acted as an attractive candidate to perform as a support for fabrication of highly stable nanocomposite materials [22]. However, sepiolite has not been widely employed for remediating antibiotics contaminated wastewater. Thus, combining the advantages of iron oxide nanomaterials with sepiolite may obtain excellent adsorption performance by alleviating particle aggregation of iron oxide nanomaterials and forming new nanostructures as well as creating more adsorption sites [20,24]. So far, hydrothermal treatment, calcination, coprecipitation and impregnation processes were commonly applied to attach iron oxide particles on the surface of sepiolite [20,22,24–28]. However, fabrication of highly monodispersed and stable iron oxide nanomaterials modified sepiolite and its application in the highly efficient adsorption of antibiotics in the complicated environmental wastewater are still challenging. Accordingly, developing a facile method for preparing highly monodispersed iron oxide nanoparticles modified sepiolite composites with controllable morphology and high activity is necessary.

Herein, highly dispersed Fe_3O_4 nanoparticles modified sepiolite composite (Fe_3O_4-sep-vacuum) was synthesized in-situ using a facile vacuum-filtration assisted coprecipitation method for the first time. Ciprofloxacin (CIP) was selected as a model antibiotic to evaluate the adsorption performance of as-prepared composites. The effects of environmental conditions such as pH, temperature, ionic strength, ionic type and humic acid (HA) on the adsorption of CIP were systematically investigated. The stability and reusability of Fe_3O_4-sep-vacuum during CIP adsorption process were examined. The interaction mechanism between CIP and Fe_3O_4-sep-vacuum was elucidated and discussed. These results indicated that the Fe_3O_4-sep-vacuum shows a promising application in remediation of antibiotics contaminated water. Our findings could also provide new opportunities in the design and fabrication of other high activity nanoparticles modified sepiolite composites with enhanced performance in eliminating pollutants from wastewater.

2. Experimental section

2.1. Materials

Sepiolite powder, ciprofloxacin, and ofloxacin were purchased from Shanghai Aladdin Biochemical Technology Co., Ltd. $Fe(NO_3)_3{\cdot}9H_2O$, $FeSO_4{\cdot}7H_2O$, NaOH, NaCl, $CaCl_2$, $MgCl_2$, $CdCl_2$, $ZnCl_2$, NaCl, $NaNO_3$, Na_2CO_3, Na_2SO_4, NaH_2PO_4, and ethanol were purchased from Shanghai Chemical Reagent Corporation, China. All reagents were of analytical reagent grade and used as received. Ultrapure water was used in the study.

2.2. Synthesis and characterization of Fe_3O_4 modified sepiolite composite

Fe_3O_4 modified sepiolite composite was prepared by a vacuum-filtration assisted coprecipitation method (Fig. 1). First, a 100 mL mixture solution containing $Fe(NO_3)_3{\cdot}9H_2O$ (1.61 g) and $FeSO_4{\cdot}7H_2O$ (0.5 g) was prepared in a vacuum chamber. Then, 2 g of dried sepiolite powder was added into the above solution, which was subsequently vacuumized using a pump for 30 min to remove air bubbles from the lumen of sepiolite. Then, the suspension was stirred for 30 min at atmospheric pressure. Subsequently, the suspension was vacuum filtered to remove the supernatant, after which 0.01 mol/L NaOH solution was added dropwise onto the solid under vigorously stirring until the solution pH reached 9. The resulting dark-brown solution was further stirred for 30 min at 60 °C. After cooling to room temperature, the resultant product was centrifuged to harvest, and fully washed with water for several times until the filtrate was neutral. Finally, the as-synthesized sample was dried at 80 °C overnight. The resultant sample was denoted as Fe_3O_4-sep-vacuum. As a reference, sepiolite loading with Fe_3O_4 nanoparticles was also prepared by conventional coprecipitation method. Briefly, 2 g of dried sepiolite powder was directly added into a 100 mL mixture solution containing $Fe(NO_3)_3{\cdot}9H_2O$ (1.61 g) and $FeSO_4{\cdot}7H_2O$ (0.5 g). Then, 0.01 mol/L NaOH solution was added dropwise into the solution under vigorously stirring until the solution pH reached 9, after which the solution was treated using a procedure similar to that for the Fe_3O_4-sep-vacuum. The obtained composite was denoted as Fe_3O_4-sep-coprecipitation. Fe_3O_4 nanoparticles were prepared by traditional coprecipitation method without adding sepiolite using an identical procedure to that for the Fe_3O_4-sep-coprecipitation. The crystal phase composition and crystallinity were characterized using X-ray diffraction (XRD, Empyrean, PANalytical B·V, Netherlands) operating with Cu-Kα radiation and a scanning rate of 2 °/min. The morphologies of samples were observed using transmission electron microscope (TEM, Tecnai G2 F20 S-Twin, FEI Company, Hillsboro, OR, USA) with an accelerating voltage of 200 kV and Field emission scanning electron

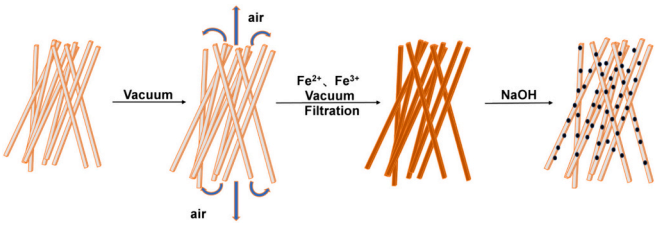

Fig. 1. Schematic for the fabrication of Fe_3O_4 nanoparticles modified sepiolite composite using a vacuum-filtration assisted coprecipitation method.

microscopy (FESEM, Scios, FEI Company, USA) with an acceleration voltage of 30.0 kV. The zeta potentials of samples were measured using a multi angle particle size and high sensitive zeta potential analyzer (Omni, Brookhaven, USA). The multi-point BET (Brunauer–Emmett–Teller) model and Barrett-Joyner-Halenda (BJH) method were used to analyze the specific surface area and pore-size distribution by a nitrogen adsorption apparatus (Autosorb-iQ2-MP, Quantachrome). The attenuated total reflectance-Fourier transform infrared spectroscopy (ATR-FTIR, Vertex 70 spectrometer, BRUKER OPTICS, US) was used to characterize the surface functional groups of the samples in the wavelength range 4000–400 cm^{-1}, and the ATR-FTIR scan time of the samples was maintained at 32 scans. X-ray photoelectron Spectrometry (XPS) was performed using a K-Alpha X-ray photoelectron spectrometer (Thermo Fisher Scientific, UK) with a monochromatic Al Kα X-ray source (excitation energy = 1468.6 eV), and binding energies were corrected relative to the carbon 1 s signal at 284.8 eV. Thermogravimetric analysis (TG) and differential scanning calorimetry (DSC) measurements were conducted in a static air atmosphere at a heating rate of 0.5 °C/min using a thermal analysis apparatus (STA 449 F3 Jupiter, Selb, Germany). ^{57}Fe Mössbauer spectroscopy was used at room temperature in the transmission mode operating in constant acceleration mode using a Silver Double Limited WSS-10 spectrometer. A ^{57}Co in the Rh matrix was used as the Mössbauer source. The velocity drive transducer was operated in a triangular waveform mode over energy ranges of ±15 mm/s. The spectrometer was calibrated using standard α-Fe foil.

2.3. Adsorption experiments of CIP

CIP was chosen to determine adsorption performance of as-prepared Fe_3O_4 modified sepiolite composites. Reaction solution was operated at room temperature and stirred throughout the experiment with a magnetic stirrer. In a typical adsorption experiment, Fe_3O_4 modified sepiolite composites (0.1 g) was added into solution (100 mL) containing CIP with various concentrations and initial pH. About 5 mL of solution was sampled at different time intervals and filtered with 0.45 μm Millipore filter for further analysis. The residual aqueous concentrations of CIP were analyzed by ultraviolet-visible spectrophotometry (UV-VIS, Cary 300, Agilent) at a wavelength of 272 nm. The difference between the initial concentrations (C_0, mg/L) and residual aqueous concentrations (C, mg/L) of CIP at a given time was used to calculate the adsorption extent of CIP. The C/C_0 against the time (t) was used for plotting the normalized adsorption curves. The adsorption amount (q, mg/g) of CIP per gram of adsorbent was calculated as the following Eq. [29]:

$$q_t = (C_0 - C) \times V/m \quad (1)$$

where V (L) is the volume of solution, m (g) is the amount of adsorbent in CIP solution.

2.4. Stability and reusability test

In the stability and reusability test experiment, 20 mg/L CIP (100 mL) was initially adsorbed by Fe_3O_4-sep-vacuum (0.1 g) at initial pH 6.0, followed by desorption using ethanol for 4 h at room temperature. Then the Fe_3O_4-sep-vacuum was dried and reused for further adsorption/desorption cycle test.

3. Results and discussion

3.1. Structure and morphology properties of prepared Fe_3O_4 modified sepiolite composites

Typical TEM images of sepiolite (Fig. 2a), Fe_3O_4 (Fig. 2b), Fe_3O_4-sep-

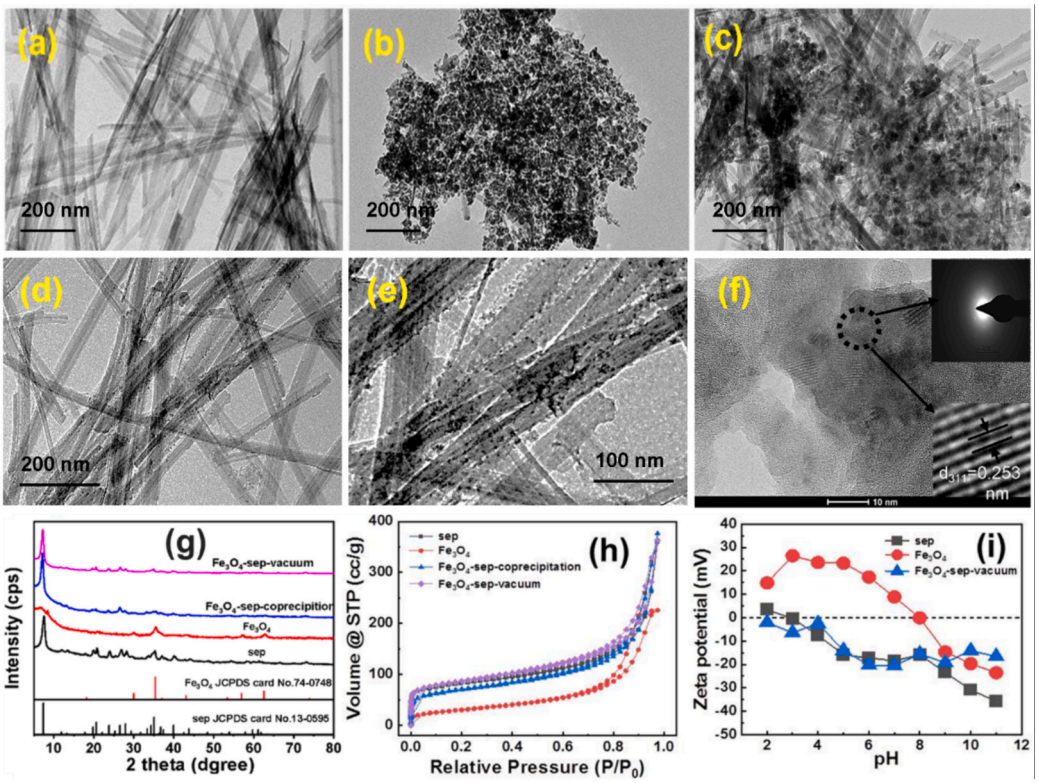

Fig. 2. Low-magnification TEM image of sepiolite (**a**), Fe_3O_4 (**b**), Fe_3O_4-sep-coprecipitation (**c**), and Fe_3O_4-sep-vacuum (**d**); (**e**) The enlarged TEM image of Fe_3O_4-sep-vacuum; (**f**) high-magnification TEM (HR-TEM) image with the corresponding fast Fourier transformed (FFT) pattern of lattice fringing pattern of Fe_3O_4-sep-vacuum; (**g**) XRD patterns of samples; (**h**) The nitrogen adsorption-desorption isotherms for sepiolite, Fe_3O_4, Fe_3O_4-sep-coprecipitation, and Fe_3O_4-sep-vacuum; (**i**) zeta potential values of sepiolite, Fe_3O_4, and Fe_3O_4-sep-vacuum at different pHs.

coprecipitation (Fig. 2c), and Fe_3O_4-sep-vacuum (Fig. 2d-f) are demonstrated in Fig. 2. The pristine sepiolite exhibited fiber-like morphology with a smooth surface and consisted of many crystal bundles. Pure Fe_3O_4 sample exhibited significant agglomeration, which is consisted of irregular nanoparticles with a size of about 100 nm. The TEM image of the sample of Fe_3O_4-sep-vacuum clearly shows that a large number of small and monodispersed Fe_3O_4 nanoparticles were uniformly decorated on the surface of sepiolite fibers without obvious stack and aggregation, in which the average size of Fe_3O_4 nanoparticles was about 5 nm. The interface of Fe_3O_4 nanoparticles closely connected with the interface of sepiolite, leading to the rough surface of sepiolite. The enlarged TEM image (Fig. 2e) further verifies this result. The HRTEM image (Fig. 2f) recorded from Fig. 2e indicates a well-crystalline nature with a lattice fringes spacing of ca. 0.253 nm, corresponding to (311) crystallographic interplanar distances of magnetite Fe_3O_4. This result suggests the particles on the surface of sepiolite are magnetite Fe_3O_4 nanoparticles. The EDS result (Fig. S1) further demonstrates the existence of ~1.2 wt% Fe element in this sample. It should be noted that most Fe_3O_4 nanoparticles were uniformly distributed on the surface of sepiolite fibers, indicating that the highly monodispersed Fe_3O_4 nanoparticles modified sepiolite composite has been successfully synthesized. For comparison, the sample of Fe_3O_4-sep-coprecipitation synthesized using conventional coprecipitation method was also investigated. As shown in Fig. 2c, obvious agglomeration of Fe_3O_4 particles with an average size of ~100 nm were observed, and most of Fe_3O_4 particles were not loaded on the surface of sepiolite. Deduced from above results, construction of Fe_3O_4 modified sepiolite composites via the vacuum-filtration assisted coprecipitation method can effectively improve the dispersibility and markedly alleviate the agglomeration of Fe_3O_4 nanoparticles.

Fig. 2g shows the XRD patterns of samples. The diffraction peaks at $2\theta = 7.5°$, 19.9°, 20.7°, 23.9°, 26.9°, 28.2°, 35.3°, 37.02°, and 40.0° can be attributed to the (110), (060), (131), (260), (080), (331), (371), (222), and (541) planes of sepiolite (JCPDS card No. 13–0595), respectively. The peaks at 30.2, 35.3, 43.4, and 62.9° were attributed to the (220), (311), (511), and (440) planes of Fe_3O_4 (JCPDS card No. 19–0629) with a typical face-centered cubic phase, respectively, which is in good agreement with HRTEM analysis result (Fig. 2f) [20]. Similar diffraction peaks are observed over Fe_3O_4-sep-vacuum, Fe_3O_4-sep-coprecipitation, and sepiolite, indicating that the Fe_3O_4 nanoparticles loading did not destroy the crystalline structure of sepiolite. There is a slight left shift of the diffraction peak at 7.5° for Fe_3O_4-sep-vacuum and Fe_3O_4-sep-coprecipitation as compared to sepiolite, suggesting that Fe_3O_4-coating process caused slight structural changes in the sepiolite sample. The trace of Fe_3O_4 cannot be detected in the XRD patterns of these two Fe_3O_4 nanoparticles modified sepiolite composites, which may be due to the ultra-fine sizes of Fe_3O_4 nanoparticles and the low content of Fe_3O_4 in these composites. Furthermore, the FTIR spectra of sepiolite, Fe_3O_4, and Fe_3O_4-sep-vacuum (Fig. S2) also showed that ultra-fine sizes and low content of Fe_3O_4 nanoparticles did not change the characteristic absorption peaks of sepiolite. Mössbauer spectra for Fe_3O_4, Fe_3O_4-sep-coprecipitation, and Fe_3O_4-sep-vacuum were shown in Fig. S3. The Mössbauer spectra for Fe_3O_4 can be deconvoluted into one doublet and two sextets. Doublet indicates that part of Fe_3O_4 nanoparticles might be superparamagnetic. Two sextets represent site A with a tetrahedral space formed by Fe(III), and site B with an octahedral space formed by Fe(II) and Fe(III). In comparison, the isomer shift for site A and B was observed for Fe_3O_4-sep-coprecipitation, implying the bond length between Fe—Fe in Fe_3O_4 might be shortened and the interaction enhanced [30]. Furthermore, for Fe_3O_4-sep-vacuum, only slight signal of doublet was observed due to ultra-fine sizes and low content of Fe_3O_4 nanoparticles in this sample.

The nitrogen adsorption-desorption isotherms for sepiolite, Fe_3O_4, Fe_3O_4-sep-coprecipitation, and Fe_3O_4-sep-vacuum were shown in Fig. 2h. The adsorption-desorption isotherm of all samples were close to a type IV isotherm with a H3 hysteresis loop in the range of P/P_0 0.7–1.0, suggesting the presence of mesoporous structure in these samples [31]. This should be ascribed to the presence of abundant nanoporous structural cavities of tunnels and channels in a cross-section of sepiolite, and the mesoporous structure of Fe_3O_4 sample was due to the inter-particle pores packing from the agglomeration of Fe_3O_4 nanoparticles [32]. The loading of Fe_3O_4 nanoparticles via vacuum-filtration assisted coprecipitation method rarely affected the microporous structure of sepiolite. Compared with sepiolite and Fe_3O_4-sep-vacuum, Fe_3O_4-sep-coprecipitation exhibit weakened hysteresis loops, implying the diminishment of some pores in Fe_3O_4-sep-coprecipitation composites due to the filling of the original micropores of sepiolite by Fe_3O_4. The BET surface area of sepiolite calculated by Barrett–Joyner–Halenda (BJH) method was 297.763 m^2/g, and it was decreased to 249.053 m^2/g for Fe_3O_4-sep-coprecipitation, which further confirms the partly blocking of inner pores and tunnels of sepiolite by Fe_3O_4 nanoparticles [33]. Fe_3O_4 nanoparticles exhibited the lowest BET surface area (111.584 m^2/g) due to its high density as well as severe agglomeration. Fe_3O_4-sep-vacuum exhibited the highest BET surface area (313.810 m^2/g), which is higher than those of sepiolite and Fe_3O_4-sep-coprecipitation, suggesting that the loading of small Fe_3O_4 nanoparticles on sepiolite surface might bring about some smaller pores. The larger specific surface area implies more adsorption sites and higher adsorption performance, which would be beneficial for adsorbing antibiotic pollutants [34].

Thermogravimetric analysis (TG) and differential scanning calorimetry (DSC) curves of sepiolite, Fe_3O_4, Fe_3O_4-sep-coprecipitation, and Fe_3O_4-sep-vacuum were shown in Fig. S4. Thermal analysis data for sepiolite and Fe_3O_4 demonstrated mass losses by 27.5 % and 10 % in the temperature ranges 600–760 °C and 30–350 °C, respectively. These mass losses correspond to the removal of structural –OH groups of sepiolite and water in Fe_3O_4, respectively. The exothermal peak at 737 °C for sepiolite could be assigned to the phase transformation of sepiolite to enstatite ($MgSiO_3$) [25]. The results of TG and DSC of Fe_3O_4-sep-coprecipitation and Fe_3O_4-sep-vacuum composites showed the presence of the mass loss characteristic for both parent materials in the temperature ranges 30–350 °C and 600–760 °C, indicating water removal in Fe_3O_4 and the phase transformation of sepiolite to enstatite. Furthermore, compared to Fe_3O_4-sep-coprecipitation, lower mass loss for Fe_3O_4-sep-vacuum could be ascribed to lower quantity of Fe_3O_4 in the sample Fe_3O_4-sep-vacuum [28]. These results showed that Fe_3O_4-sep-vacuum had high thermal stability.

Fig. 2i illustrates the zeta potential values of sepiolite, Fe_3O_4, and Fe_3O_4-sep-vacuum at different pHs. For Fe_3O_4, an isoelectric point (pH_{IEP}) value of about 8.0 was detected. This suggests that at pH values lower than 8.0, the Fe_3O_4 surface is positively charged, while it is negatively charged at pH >8.0. The zeta potential values of sepiolite and Fe_3O_4-sep-vacuum were negative when pH values ranged from 2 to 11, indicating these samples are negatively charged at all tested pH conditions. With increasing pH, their zeta potential became increasingly more negative, indicating higher surface negative charge densities of these samples at higher pH. Only subtle differences in the zeta potential values of sepiolite and Fe_3O_4-sep-vacuum could be observed, suggesting that trace of Fe_3O_4 had insignificant effect on the zeta potential values of sepiolite.

As described in the experimental section, during the process of conventional coprecipitation method, Fe^{3+} and Fe^{2+} would be co-precipitated by adding OH^- to form Fe_3O_4 nanoparticles in solution. The zeta potential of pure Fe_3O_4 nanoparticles and sepiolite (Fig. 2i) at pH 9.0 was −15 and − 22 mV, respectively, implying that both Fe_3O_4 nanoparticles and sepiolite are negatively charged, which provides enough electrostatic repulsion to hinder Fe_3O_4 nanoparticles to adsorb on the surface of sepiolite. Therefore, the conventional coprecipitation method is unable to prepare monodispersed Fe_3O_4 nanoparticles modified sepiolite composites with uniform size. Conversely, the vacuum treatment process for sepiolite could remove air bubbles from the lumen of sepiolite, which facilitates the solution to enter by pulling and breaking vacuum, and thus positive charged Fe^{3+} and Fe^{2+} could be

preferentially adsorbed and accumulated on the surface and filled in the lumen of sepiolite with negatively charged sites to saturation through the double layer charge effects (Fig. 1). Most of supernatant which contains residual Fe^{3+} and Fe^{2+} would be removed by subsequent vacuum filtration treatment, while Fe^{3+} and Fe^{2+} adsorbed on the surface and filled in the lumen of sepiolite would be maintained due to the electrostatic interaction and capillary force. The adsorbed and filled Fe^{3+} and Fe^{2+} will be converted into Fe_3O_4 with the addition of OH^-, and further nucleate and grow in situ into Fe_3O_4 nanoparticles on the surface of sepiolite, eventually yielding the monodispersed Fe_3O_4 nanoparticles modified sepiolite composites. The sizes of the Fe_3O_4 nanoparticles on the surface of sepiolite prepared via the vacuum-filtration assisted coprecipitation method are significantly smaller than the sample synthesized by conventional coprecipitation method. This can be ascribe to that the low amount of Fe^{3+} and Fe^{2+} adsorbed on the surface and filled in the lumen of sepiolite limits the growth of Fe_3O_4 nanoparticles, hindering their coagulation to larger particles, leading to a small size and good dispersibility of Fe_3O_4 nanoparticles on the surface of sepiolite. Based on the above results, it can be concluded that the vacuum-filtration assisted coprecipitation method could be used to in-situ prepare monodispersed Fe_3O_4 nanoparticles modified sepiolite composites with a small and uniform size in comparison with the conventional coprecipitation method.

3.2. Adsorption performance of different samples for CIP

Fig. 3 shows the adsorption curves of 20 ppm CIP with an initial pH of 6.0 by sepiolite, Fe_3O_4, Fe_3O_4-sep-coprecipitation, and Fe_3O_4-sep-vacuum. For the pure Fe_3O_4 nanoparticles and sepiolite, only approximately 56 % and 80 % of CIP was adsorbed after 120 min, respectively. Furthermore, an adsorption experiment in a suspension mixing of pure sepiolite and Fe_3O_4 with equivalent mass was also carried out, and approximately 69 % CIP was adsorbed after 120 min. Comparatively, the samples of Fe_3O_4-sep-coprecipitation and Fe_3O_4-sep-vacuum exhibited significantly higher CIP removal efficiencies than those of pure Fe_3O_4 nanoparticles and sepiolite. Fe_3O_4-sep-vacuum exhibited the highest CIP removal rate, by which about 93 % of CIP was removed within 60 min, suggesting that Fe_3O_4-sep-vacuum had dramatically higher CIP removal capacity than Fe_3O_4-sep-coprecipitation. CIP was rapidly absorbed by the Fe_3O_4-sep-vacuum at beginning 2 min, which may be due to the rapid diffusion of CIP from the solution to the external surfaces of Fe_3O_4-sep-vacuum. After about 20 min, adsorption equilibrium reached, indicating that the adsorption process of CIP is a complex process, which probably contains intra-particle diffusion, surface complexation and film diffusion [35]. This might be related to that Fe_3O_4-sep-vacuum with small size and good dispersibility of Fe_3O_4 nanoparticles on the surface of sepiolite had the highest BET surface area (313.810 m^2/g) and more adsorption sites, which facilitates the removal of CIP via adsorption, leading to its highest adsorption performance for CIP. Furthermore, the adsorption of CIP by all samples could reach equilibrium within 60 min. It should be noted that although Fe_3O_4-sep-coprecipitation (249.053 m^2/g) had lower specific surface area than that of sepiolite (297.763 m^2/g), Fe_3O_4-sep-coprecipitation exhibited higher CIP removal efficiencies than sepiolite, implying that the enhanced adsorption ability for CIP should be resulted from the contribution of Fe_3O_4.

The adsorption kinetic curve of CIP by Fe_3O_4-sep-vacuum was fitted using pseudo-first-order, pseudo-second-order and intraparticle diffusion kinetic models. The three models were respectively expressed by eq. (2), (3), and (4) as follow [18,29]:

$$ln(q_e - q_t) = lnq_e - k_1 t \quad (2)$$

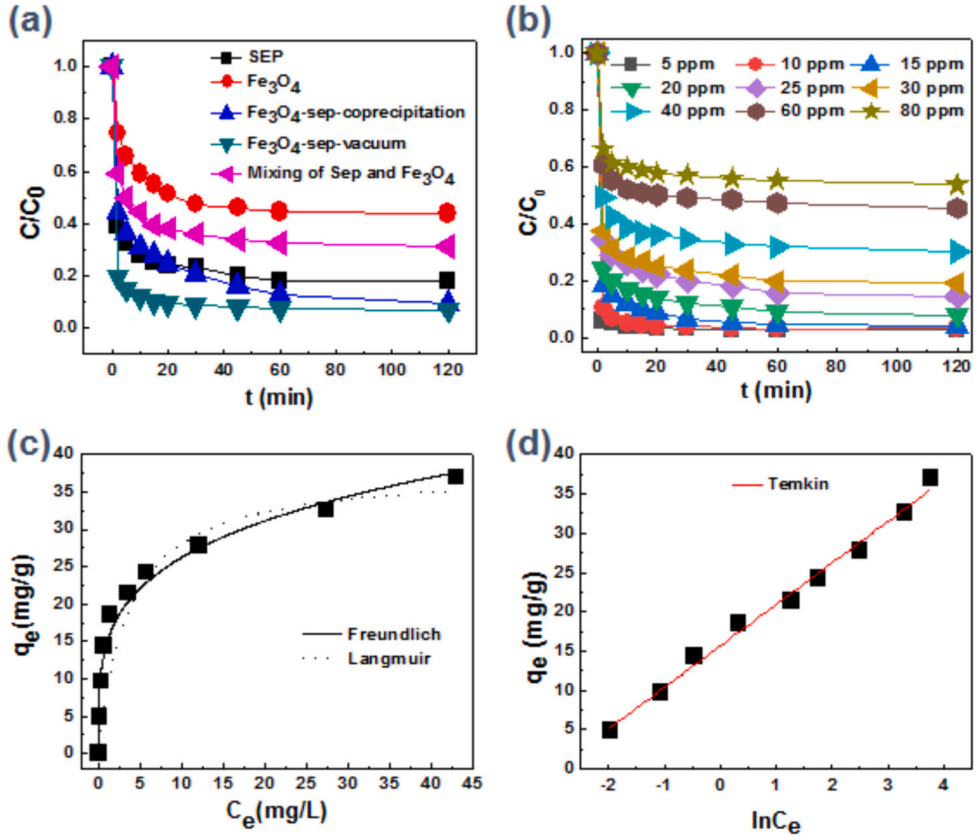

Fig. 3. (**a**) The adsorption curves of 20 ppm CIP by sepiolite, Fe_3O_4, Fe_3O_4-sep-coprecipitation, Fe_3O_4-sep-vacuum, and mixing of sepiolite and Fe_3O_4; (**b**) Adsorption of different concentrations of CIP by Fe_3O_4-sep-vacuum; (**c**) Fitting of adsorption isotherms of CIP through Freundlich and Langmuir models; (**d**) Fitting of adsorption isotherms of CIP through Temkin model. Experimental conditions: samples = 1 g/L, T = 25 °C, pH = 6.

$$t/q_t = t/q_e + 1/(k_2\, q_e^2) \quad (3)$$

$$q_t = k_{dif}\, t^{1/2} + C \quad (4)$$

where t is the reaction time (min), k_1 and k_2 are the equilibrium rate constants for pseudo-first and pseudo-second order, respectively. q_t and q_e (mg/g) are the amount of CIP deposited by per gram of Fe_3O_4-sep-vacuum at time t and at equilibrium, respectively. C is the intercept related to the boundary layer thickness (mg/g) and k_{dif} is the intra-particle diffusion rate constant (mg $min^{-1/2}$ g^{-1}). The obtained kinetic parameters and correlation coefficients (R^2) from three kinetic models for CIP adsorption are represented in Table S1 and Fig. S5. The values of R^2 obtained from the pseudo-second-order kinetic model was the highest, which was 0.9997, indicating that the pseudo-second order kinetic model might be more suitable for explaining the experimental data for CIP adsorption process by Fe_3O_4-sep-vacuum. Furthermore, the $q_{e,cal}$ (18.749 mg/g) value achieved from the pseudo-second order kinetic model is almost equal to $q_{e,exp}$ (18.4 mg/g), confirming the effectiveness of this model [18]. This indicates chemical adsorption for CIP by Fe_3O_4-sep-vacuum and no resistance to internal diffusion.

The effect of initial concentrations of CIP on the adsorption process was investigated at pH 6.0 (Fig. 3b). When the initial concentration of CIP did not exceed 15 ppm, approximately 99 % of CIP was adsorbed after 120 min. CIP could be completely removed when the initial concentration of CIP was 10 ppm or lower. With increasing initial concentrations of CIP, the equilibrium adsorption amount (q_e) of CIP gradually increased. The isotherm was fitted using Langmuir (Eq. 5), Freundlich (Eq. 6), Temkin (Eq. 7), and BET (Eq. 8) models [29]. The calculated isotherm parameters are given in Table 1 and the fitted adsorption isotherm are presented in Figs. 3c and d.

$$C_e/q_e = C_e/q_m + 1/(q_m\, K_L) \quad (5)$$

$$ln(q_e) = ln(K_F) + (1/n)\, ln(C_e) \quad (6)$$

$$q_e = B\, ln(K_T) + B\, ln(C_e) \quad (7)$$

$$C_e/q_e\,(1 - C_e) = 1/(q_m\, k) + [k1/q_m\, k)]C_e \quad (8)$$

where C_e (mg/L) is the concentration of the CIP at equilibrium; q_e and q_m (mg/g) represent the amounts of CIP at time t (min) and adsorption capacities at maximum, respectively; K_L, K_F, K_T, and k are the adsorption constants of Langmuir, Freundlich, Temkin, and BET, respectively; n is the Freundlich dimensionless empirical coefficient representing the adsorption strength. B = RT/b represents the heat of adsorption (J/mol), in which b is the Temkin constant, T (K) is the absolute temperature, and R is 8.314 J/mol K^{-1}. In Langmuir isotherm, an important dimensionless constant called the equilibrium parameter (R_L) was defined by $R_L = 1/(1 + K_L C_0)$, where C_0 is the initial concentration of CIP [29]. The correlation coefficient (R^2) obtained from the Temkin isotherm model ($R^2 = 0.9902$) was the highest as compared to the Langmuir, Freundlich and BET isotherm models, indicating that Temkin isotherm model could better describe the adsorption behavior of CIP. This result suggests that a multilayer adsorption feature of CIP on heterogeneous energy distribution of the sorption sites on Fe_3O_4-sep-vacuum surface, on which positively charged Fe_3O_4 nanoparticles and negatively charged sepiolite are simultaneously contained at pH 6.0 [36]. Hence, it was confirmed that physisorption mechanism was involved in the adsorption process of CIP. Furthermore, the simultaneous possession positively and negatively charged groups of the zwitterionic CIP at pH 6.0 also facilitates their multilayer adsorption on Fe_3O_4-sep-vacuum surface, and thus maximizing the adsorption capacity. Therefore, based on the above kinetic and isotherm results, it can be concluded that a combination of chemisorption and physisorption of CIP on Fe_3O_4-sep-vacuum surface might take place [37].

Table 1
The adsorption isotherm parameters of CIP by Fe_3O_4-sep-vacuum.

Isotherm	Equation	Parameters	
Langmuir	$C_e/q_e = C_e/q_m + 1/(q_m K_L)$	q_m (mg/g)	38.06
		K_L (L/mg)	3.57
		R^2	0.8957
		R_L	0.0035–0.053
Freundlich	$\ln(q_e) = \ln(K_F) + (1/n)\ln(C_e)$	n	4.042
		K_F (mg/g.(L/mg)$^{1/n}$)	14.83
		R^2	0.9742
Temkin	$q_e = B\ln(K_T) + B\ln(C_e)$	b (J/mol)	469.5128
	$B = RT/b$	K_T (L/g)	19.4096
		R^2	0.9902
BET	$C_e/q_e\,(1\text{-}C_e) = 1/(q_m k) + [(k\text{-}1/q_m k)]C_e$	q_m (mg/g)	–
		K	–
		R^2	0.814

3.3. Adsorption of CIP by Fe_3O_4-sep-vacuum at different conditions

3.3.1. Effect of pH

The surface charges of solid materials and chemical speciation of ionizable antibiotics with various functional groups in solution are dominated by solution pH, which often plays the most crucial role in controlling the transport and fate of ionizable antibiotics, and thus has a decisive influence on their adsorption efficiencies. Hence, the effect of solution initial pH (2.0–13.0) on the adsorption of CIP by Fe_3O_4-sep-vacuum was systematically investigated, and the experiments were carried out in system containing CIP (20 mg/L), Fe_3O_4-sep-vacuum (1 g/L) at different initial pHs. Fig. 4a shows that the adsorption of CIP was highly pH dependent, and similar adsorption kinetic curves at different pHs were observed. The q_e of CIP (Fig. 4b) initially increased with pH value increased from 2.0 to 4.0 and reached a maximum at pH 4.0 and then remarkably decreased at higher pH values. When the pH value increased to 13, approximately 10 % of CIP was adsorbed. The highest adsorption rate of CIP was achieved at initial pH 4.0, and approximately 95 % of CIP could be removed within 20 min. This tendency should be related to the surface charges of Fe_3O_4-sep-vacuum as well as the existing species of CIP, which is highly depend on the solution pH. The zeta potential values of Fe_3O_4-sep-vacuum were negative at all tested pH conditions, indicating its surface was negatively charged. When solution pH increased from 2.0 to 4.0, the zeta potential of the Fe_3O_4-sep-vacuum kept minor change, while it sharply declined with further increasing solution pH from 4.0 to 6.0. Increasing pH would lead to a greater extent of deprotonation of surface groups on Fe_3O_4-sep-vacuum and more negative charges on its surface because its pH_{IEP} was lower than 2.0. At the same time, CIP molecule contains one acidic and one basic group, whose pK_a is 6.16 and 8.23, respectively [11]. Three dissociation species, including positively charged ($HCIP^+$), zwitterionic ($CIP^{\pm}$), and negatively charged (CIP^-) species, would be existed at different pHs. At low pH values, cationic specie of $HCIP^+$ is the dominant form of CIP, the competition between cationic species of $HCIP^+$ and H^+ for adsorption sites on Fe_3O_4-sep-vacuum surface would lead to the decreased adsorption of CIP. As pH increased to 4.0, almost all CIP molecules are present in cationic species, but the concentration of H^+ significantly decreased, thus adsorption efficiency reached the highest. With further increasing pH, deprotonated species become more dominant due to hydrolysis of CIP. In the pH range from 6.16 to 8.23, zwitterions of $CIP^{\pm}$ is the dominant dissociation species of CIP, in which amine functional groups are present in the form of $=NH_2^+$ and carboxyl functional groups can be found in the form of $-COO^-$ [4,16]. The weakened electrostatic interaction and enhanced hydrophobic interaction will primarily contribute to the adsorption of CIP. At high pH values, both the anionic carboxylate group of CIP and the surface sites of Fe_3O_4-sep-vacuum are significantly negative charged, resulting in low equilibrium adsorption amount of CIP due to the electrostatic repulsion between them.

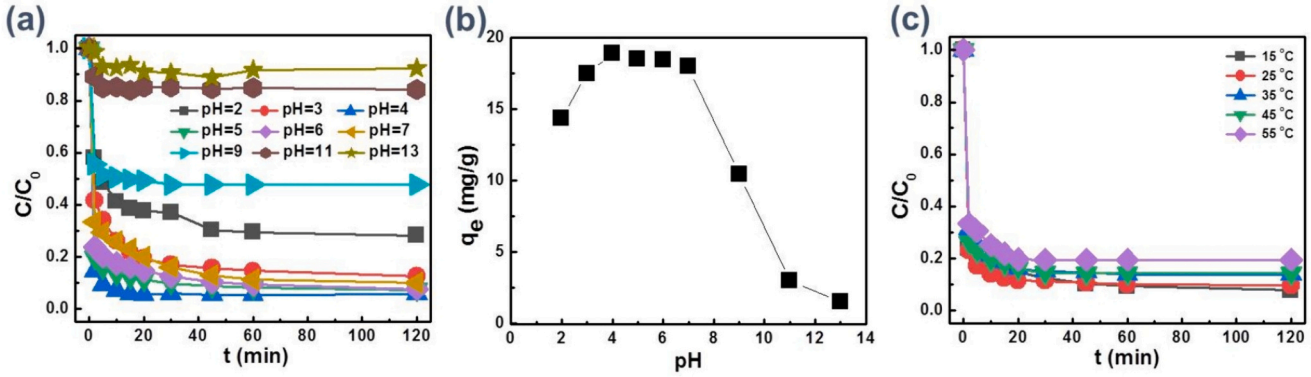

Fig. 4. (**a**) Effect of pH on adsorption of CIP; (**b**) The equilibrium adsorption amount (q_e) of CIP at different pHs; (**c**) Effect of Temperature on adsorption of CIP. Experimental conditions: Fe_3O_4-sep-vacuum = 1 g/L, CIP = 20 ppm.

3.3.2. *Effect of temperature*

Temperature is expected to influence the adsorption behavior of CIP on Fe_3O_4-sep-vacuum surface and thus was investigated (Fig. 4c). With increasing temperature from 20 to 60 °C, the adsorption efficiencies of CIP decreased monotonously from about 93 % to 80 % after 120 min. This phenomenon indicates that the high temperature is not conducive to the adsorption removal of CIP, implying that the adsorption process of CIP should be an exothermic process. Higher temperature could enhance the Brownian motion and kinetic energy of adsorbent and adsorbate, which is favorable for the collision frequency and adsorption of CIP with Fe_3O_4-sep-vacuum surface. However, hydrogen bonding interaction would decrease with enhancing temperature, which could reduce adsorption of CIP with Fe_3O_4-sep-vacuum surface.

3.3.3. *Effect of ionic strength and ionic type*

Various cations and anions with different concentrations universally exist in estuarine and coastal waters as well as various wastewaters, and thus might affect the removal of antibiotics in real aquatic environments. To thoroughly understand the influence of ionic strength and ionic type on the adsorption of CIP (20 ppm) by Fe_3O_4-sep-vacuum, various representative cations (NaCl, $CaCl_2$, $MgCl_2$, $CdCl_2$, and $ZnCl_2$) and anions (NaCl, $NaNO_3$, Na_2CO_3, Na_2SO_4, or NaH_2PO_4) with different concentrations and valences were added into the solution.

The influence of ionic strength on the adsorption of CIP by Fe_3O_4-sep-vacuum was studied by adding different concentrations of NaCl at an initial pH of 6.0. As shown in Fig. 5a, with increasing NaCl concentrations from 0 to 1000 mM, the adsorption efficiencies of CIP significantly decreased from about 93 % to 60 %. This may be ascribed to that increasing ionic strength can reduce the electrostatic attractive forces between CIP and Fe_3O_4-sep-vacuum owing to the decreased thickness of electrostatic double layer of Fe_3O_4-sep-vacuum, leading to the decrease in the adsorption of CIP. Furthermore, high concentration of Na^+ ion would compete the active adsorptive sites on surface of Fe_3O_4-sep-vacuum with CIP, resulting in the decreased adsorption of CIP. This result highlights the crucial role of electrostatic interaction in adsorption of CIP by Fe_3O_4-sep-vacuum.

The effect of ionic type on the adsorption of CIP by Fe_3O_4-sep-vacuum was also investigated by adding 10 mM cations (Fig. 5b) and anions (Fig. 5c) at an initial pH of 6.0. The result shows that the addition of anions and cations especially divalent cations markedly reduced CIP

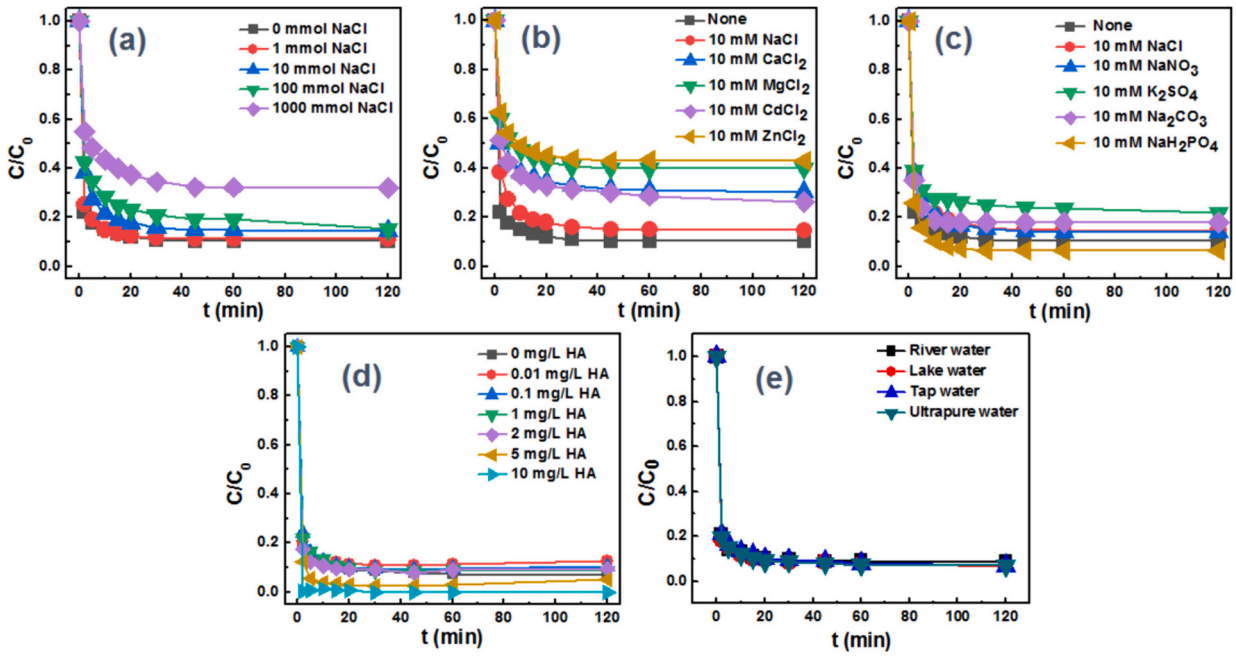

Fig. 5. (**a**) The influence of ionic strength (different concentrations of NaCl) on the adsorption of CIP; Effect of ionic type on the adsorption of CIP: 10 mM cations (**b**) and anions (**c**); (**d**) Effect of HA concentration (0–10 ppm) on the adsorption of CIP; (**e**) The adsorption of CIP in indifferent real water samples. Experimental conditions: Fe_3O_4-sep-vacuum = 1 g/L, CIP = 20 ppm, pH = 6, T = 25 °C.

adsorption capacity. For instance, without the presence of ions, approximately 93 % of CIP could be removed after 120 min. With the addition of NaCl, $CaCl_2$, $MgCl_2$, $CdCl_2$, or $ZnCl_2$, approximately 85 %, 71 %, 60 %, 73 %, and 57 % of CIP was removed after 120 min, respectively. Divalent cations showed higher inhibitory effects on the adsorption of CIP by Fe_3O_4-sep-vacuum than monovalent cations, attributing to more significant compression of electric double layer of Fe_3O_4-sep-vacuum by divalent ions in comparison to monovalent ions. According to the Derjaguin–Landau–Verwey–Overbeek (DLVO) theory, cations with the same valence would have parallel abilities to neutralize surface negative charges of Fe_3O_4-sep-vacuum, implying that divalent cations would exhibit stronger capacities to neutralize surface negative charges of Fe_3O_4-sep-vacuum than monovalent cations. With the addition of NaCl, $NaNO_3$, Na_2CO_3, or Na_2SO_4, approximately 85 %, 85 %, 82 %, and 78 % of CIP was removed after 120 min, respectively, indicating that these anions had slight effect on the adsorption of CIP. However, in the presence of NaH_2PO_4, 96 % of CIP was removed after 120 min. The special interaction between $H_2PO_4^-$ (the existence form of phosphate at pH 6.0) and Fe_3O_4 of Fe_3O_4-sep-vacuum could penetrate the electric double layer (EDL) more easily and form complex with the surface of Fe_3O_4 in the sample of Fe_3O_4-sep-vacuum, resulting in more negative surface charges of Fe_3O_4-sep-vacuum. This would increase electrostatic attraction between positively charged $HCIP^+$ and negatively charged Fe_3O_4 surface in the presence of NaH_2PO_4, and thus enhancing CIP adsorption [38].

3.3.4. Effect of humic acid

Natural organic matter (e.g. humic substances) is a ubiquitous and abundant constituent in Earth's surface environment with concentrations ranging from sub ppm levels to tens of ppm [39], which will coexist with antibiotics in natural water and wastewater, and may significantly affect the removal of antibiotics. Fig. 5d shows the effect of HA concentration (0–10 ppm) on the adsorption of CIP (20 ppm) by Fe_3O_4-sep-vacuum at pH 6.0. As shown, the adsorption efficiency for CIP was hardly affected by low concentration HA (<2 ppm). With further increased HA concentration, CIP adsorption capacity markedly increased. For instance, with addition of 10 ppm HA, CIP could be thoroughly removed after only 2 min, suggesting that high HA concentration could accelerate the removal of CIP by Fe_3O_4-sep-vacuum. HA can be adsorbed onto Fe_3O_4-sep-vacuum surface by the interaction between ≡Fe–OH on Fe_3O_4-sep-vacuum surface and oxygen containing functional groups (–COOH and –OH) or amino groups of HA, forming inner-sphere complexes by electrostatic interaction, hydrogen bonding or ligand exchange/surface complexation, which will modify the surface physicochemical properties and reactivity of Fe_3O_4-sep-vacuum, thus affecting the adsorption behavior of CIP [40]. The adsorbed HA molecules on Fe_3O_4-sep-vacuum surface could provide additional adsorption sites for adsorbing CIP and act as a “bridge” between the Fe_3O_4-sep-vacuum surface and CIP, which benefits the adsorption and removal of CIP [41].

To explore the application of Fe_3O_4-sep-vacuum composite in real wastewater, the adsorption of CIP in indifferent real water samples, including tap water, lake water (total organic carbon/TOC = 17.83 mg/L), and river water (TOC = 46.44 mg/L), was also conducted. As shown in Fig. 5e, the adsorption efficiency for CIP in three actual water samples showed no significant change compared with that of ultrapure water. Thus, the Fe_3O_4-sep-vacuum composite can be used as a promising material for highly efficient removing CIP in natural water and wastewater containing high concentration organic matter.

3.4. Adsorption mechanism of CIP by Fe_3O_4-sep-vacuum

Based on above results, it can be concluded that electrostatic interactions play a decisive role in the adsorption process of CIP by Fe_3O_4-sep-vacuum. The adsorption extent of CIP on the surface of Fe_3O_4-sep-vacuum is mainly affected by the chemical speciation of CIP and the charge type of Fe_3O_4-sep-vacuum surface, which are significantly influenced by the solution pH. However, it should be noted that although all surface hydroxyl and carboxyl groups for both Fe_3O_4-sep-vacuum and CIP were negatively charged under solution pH > 9.0, and thereby CIP and Fe_3O_4-sep-vacuum were expected to electrostatically repel each other, approximately 52 %, 16 %, and 10 % of CIP could still be adsorbed at pH 9.0, 11.0, and 13.0, respectively. This indicates that electrostatic interaction alone cannot explain the decreased concentration of CIP in the solution in relatively high pH.

To confirm the contribution of hydrogen bonding interactions to CIP adsorption, 5 mol/L urea was added during the CIP adsorption processes. Urea is generally used as a hydrogen bond breaker to break hydrogen bonds because it can act as both acceptor and donor of hydrogen bonds for competing hydrogen bonding sites. Thus, it could destroy the original hydrogen bonding between CIP and adsorbents [42]. Fig. 6 illustrates that the adsorption efficiencies of CIP were significantly inhibited by adding urea to the solution. Specifically, the adsorption efficiency of CIP within 120 min was approximately 56 %, 80 %, and 93 % by Fe_3O_4, sepiolite, and Fe_3O_4-sep-vacuum, respectively. In the presence of 5 mol/L urea, the adsorption efficiency of CIP decreased to approximately 38 %, 65 %, and 81 % by Fe_3O_4, sepiolite, and Fe_3O_4-sep-vacuum after 120 min, respectively, suggesting a significant contribution of hydrogen bonding to CIP adsorption. Hydrogen bonding likely occurred between the –C=O/–COOH/−NH/−F groups of CIP and the −OH on the surfaces of Fe_3O_4 or sepiolite [43].

To further explore the mediating roles of surface hydroxyl groups in CIP adsorption, 1 mol/L NaF was added during the CIP adsorption processes. Fig. 6 illustrates that the adsorption efficiencies of CIP were significantly inhibited by adding F^- to the solution. Specifically, approximately 56 %, 80 %, and 93 % of CIP could be adsorbed by Fe_3O_4, sepiolite, and Fe_3O_4-sep-vacuum, respectively. In the presence of 1 mol/L F^-, approximately 7.5 %, 65 %, and 55 % of CIP was adsorbed by Fe_3O_4, sepiolite, and Fe_3O_4-sep-vacuum, respectively. This suggests that the addition of F^- can markedly inhibit the adsorption of CIP. This is mainly attributed to that Fe − OH on Fe_3O_4 surface, Si-OH on the outside surface and the Mg-OH on the inner surface of sepiolite could be almost completely substituted by F^-. F^- could also strongly coordinate with ≡Fe(III) species on Fe_3O_4 surface to form uncharged and highly stable surface species $\equiv Fe_xF_x$, which can consequently decrease the adsorption efficiency of CIP on Fe_3O_4 surface. This result illustrated that –OH bonding participated in the adsorption process of CIP on Fe_3O_4-sep-vacuum surface. In addition, ATR-FTIR spectra of sepiolite, Fe_3O_4, and Fe_3O_4-sep-vacuum before and after adsorption of CIP (Fig. 7a) were analyzed. The characteristic absorption peaks of Fe_3O_4 at 1348 and 1090 cm^{-1} corresponding to –OH disappeared distinctly after adsorption of CIP, this was accompanied by the appearance of the characteristic absorption peaks of CIP, confirming that CIP macromolecule could react with the surface of Fe_3O_4. This was consistent with the results above that –OH play an important role in the adsorption of CIP on Fe_3O_4-sep-vacuum surface due to formation of hydrogen bonding [44]. Furthermore, the FTIR spectra of sepiolite and Fe_3O_4-sep-vacuum before and after adsorption of CIP were identical due to low content of Fe_3O_4 nanoparticles on the surface of sepiolite.

To better understand the adsorption mechanism of CIP by Fe_3O_4-sep-vacuum, XPS spectra of Fe_3O_4-sep-vacuum before and after adsorption of CIP were used to explore the changes in chemical valence states during the adsorption process. As shown in Fig. 7b, for the fresh Fe_3O_4-sep-vacuum, the binding energy peaks of Fe $2p_{3/2}$ at 710.08, 711.16 and 713.55 eV were attributed to the Fe(II) in octahedral sites (oct), Fe(III) in octahedral sites (oct), and Fe(III) in tetrahedral sites (tet), respectively. After adsorption of CIP, the peaks for octahedral Fe(II), octahedral Fe (III), and tetrahedral Fe(III) slightly shifted to 709.91, 710.99, and 713.42 eV, respectively, which might be ascribed to the electron transfer between Fe and negatively charged $–COO^-$ of CIP during the adsorption reaction. The deconovoluted peaks (Fe $2p_{3/2}$) of Fe(II)/Fe(III) could be calculated to be approximately 0.5 before and after adsorption of CIP,

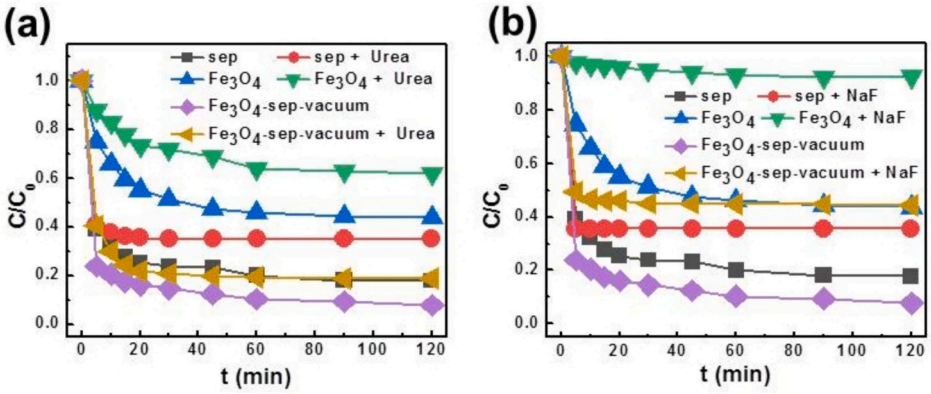

Fig. 6. (**a**) Effect of Urea (5 mol/L) on adsorption of CIP by sepiolite, Fe_3O_4, and Fe_3O_4-sep-vacuum; (**b**) Effect of NaF (1 mol/L) on adsorption of CIP by sepiolite, Fe_3O_4, and Fe_3O_4-sep-vacuum. Experimental conditions: samples = 1 g/L, CIP = 20 ppm, pH = 6, T = 25 °C.

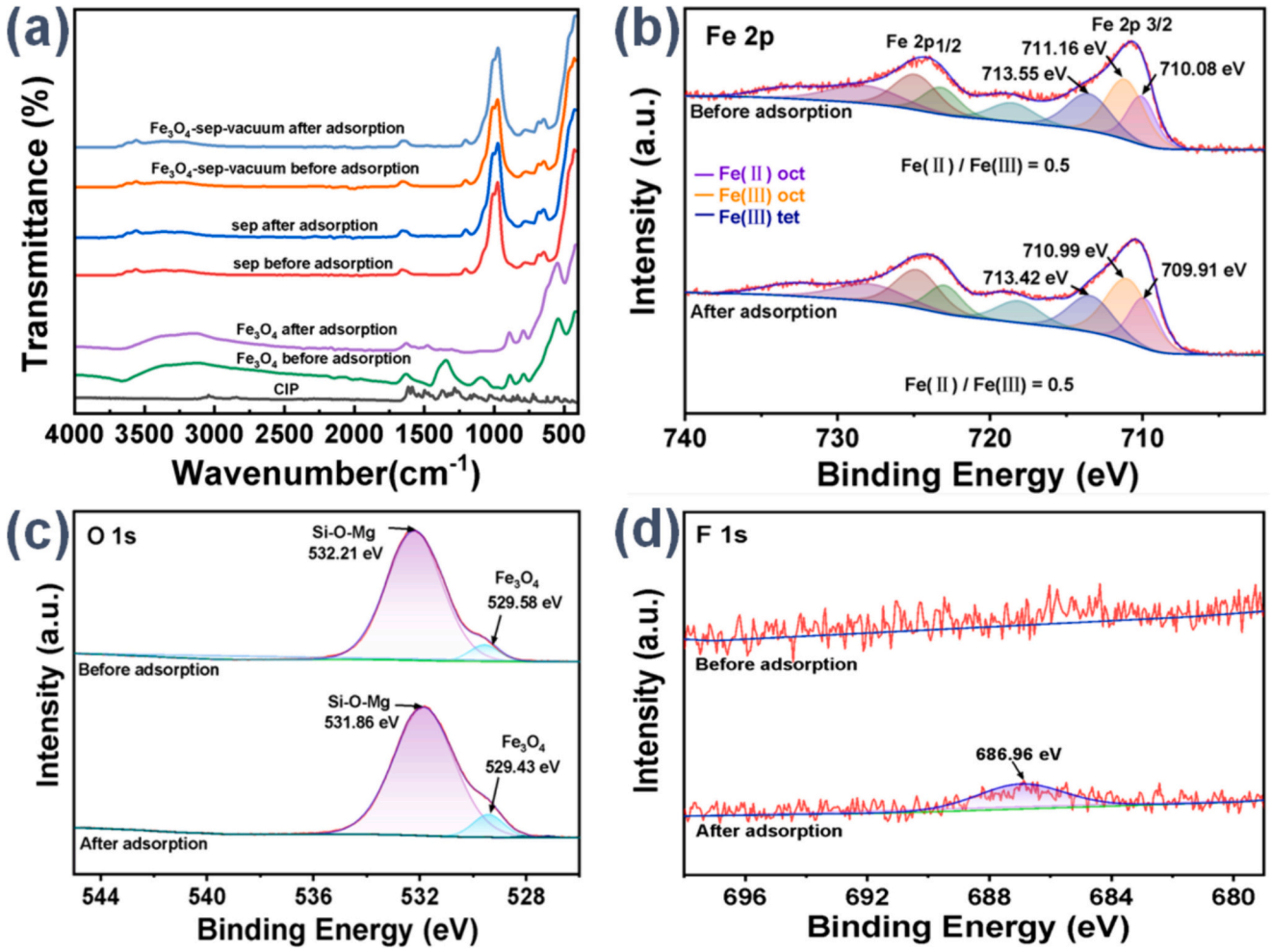

Fig. 7. (**a**) Attenuated total reflectance-Fourier transform infrared (ATR-FTIR) spectra of sepiolite, Fe_3O_4, and Fe_3O_4-sep-vacuum before and after adsorption of CIP; XPS spectra of Fe 2p (**b**), O 1 s (**c**), and F 1 s (**d**) for Fe_3O_4-sep-vacuum before and after adsorption of CIP.

which was well consistent with the stoichiometry ratio of Fe(II)/Fe(III) in Fe_3O_4, indicating that no obvious change in the surface chemical valence states of Fe for Fe_3O_4-sep-vacuum during the adsorption of CIP [20]. The O 1 s XPS spectrum (Fig. 7c) of fresh Fe_3O_4-sep-vacuum could be fitted into two components at 529.58 and 532.21 eV, which were attributed to the surface lattice oxygen (in Si-O-Mg) of sepiolite and Fe—O of Fe_3O_4, respectively. After the adsorption of CIP, the two peaks of O 1 s slightly shifted to 531.86 and 529.43 eV, respectively, indicating an increase in electron density due to the adsorption of CIP [26]. Fig. 7d shows that the peak of F 1 s at 686.96 eV can be detected on Fe_3O_4-sep-vacuum surface after the adsorption of CIP, indicating the accumulation of CIP on Fe_3O_4-sep-vacuum surface.

Therefore, based on the above discussion, various mechanisms, including electrostatic attraction, hydrogen bonding, ion exchange, surface complexation, hydrophobic interaction and van der Waals interactions between CIP and Fe_3O_4-sep-vacuum surface might contribute

to the adsorption process of CIP. A possible mechanism for adsorption of CIP on Fe_3O_4-sep-vacuum surface could be proposed and presented in Fig. 8. The carboxylate group and the neighboring carbonyl group on the quinolone ring of CIP can be hydrogen bonded with the Fe_3O_4-sep-vacuum surface. Meanwhile, a type of strong hydrogen bonds (more stronger than ordinary hydrogen bonds), which is known as negative charge-assisted hydrogen bonds ((−)CAHBs), may be formed between deprotonated hydroxyl groups on Fe_3O_4-sep-vacuum surfaces and –COOH/−NH groups of CIP, thus facilitating the adsorption of CIP by offsetting partial electrostatic repulsions. Furthermore, oxygen atoms from the carboxylate group and carbonyl group of CIP might also exchange with Fe − OH groups or directly chemically bind with Fe atoms on the Fe_3O_4-sep-vacuum surface to form inner-sphere surface complexes [15]. CIP could be adsorbed by negatively surface charged sites of Fe_3O_4-sep-vacuum surface via cation exchange with the protonated amine group [45]. CIP could also be stably immobilized inside the structural tunnels and channels in sepiolite via hydrogen bonding with the water molecules coordinated to Mg (II) ions at the edge of the octahedral sheet in the structural silicate blocks. Additionally, the reactive amino, carboxylate, carbonyl and hydroxyl groups of CIP could interact with silanol groups at the edge of sepiolite through hydrogen bonds, van der Waals interactions, and coordination bonds. Moreover, some CIP molecules could be adsorbed into the interior channels of the sepiolite to form the H-bonding interaction with zeolitic water [22]. Overall, the cumulative effect of above-mentioned forces, which are influenced by multiple factors, would determine the adsorption behavior of CIP on Fe_3O_4-sep-vacuum surface.

3.5. Stability and reusability of Fe_3O_4-sep-vacuum for removing CIP

As shown in Fig. 9a, the CIP removal efficiency was still 73.7 % after 5 cycles, indicating that the Fe_3O_4-sep-vacuum maintained excellent adsorption performance during the experiment process and has high stability and reusability. This result also suggests that the Fe_3O_4-sep-vacuum might have great application potentials in purification CIP contaminated wastewater.

3.6. Comparison of CIP removal by Fe_3O_4-sep-vacuum with various adsorbents and different antibiotics removal by Fe_3O_4-sep-vacuum

The comparison of the removal efficiency of CIP by different adsorbents, including Fe_3O_4-sep-vacuum prepared in this work and previously reported work in the literature, is listed in Table S2. As shown, Fe_3O_4-sep-vacuum exhibited excellent adsorption performance for CIP. It should be noted that both sepiolite and Fe_3O_4 are cheap, environmentally friendly, and non-toxic, and the synthesized method of Fe_3O_4-sep-vacuum is also facile. Futhermore, to explore the adaptability of Fe_3O_4-sep-vacuum composite in purifying antibiotics contaminated water, the adsorption of another antibiotic of ofloxacin (20 mg/L) was also conducted (Fig. 9b) at initial pH 6.0. Approximately 91 % of ofloxacin could be removed by Fe_3O_4-sep-vacuum after 20 min. This result showed that the Fe_3O_4-sep-vacuum could be served as a promising adsorbent in remediation of antibiotics contaminated water.

4. Conclusions

In summary, highly dispersed Fe_3O_4 nanoparticles modified sepiolite composite (Fe_3O_4-sep-vacuum) was synthesized in-situ using a facile vacuum-filtration assisted coprecipitation method for the first time. This Fe_3O_4-sep-vacuum composite exhibited significantly higher adsorption capacity to ciprofloxacin than those of pure Fe_3O_4 nanoparticles and sepiolite. Comparatively, the sample of Fe_3O_4-sep-vacuum exhibited significantly higher CIP removal efficiencies than those samples obtained by traditional coprecipitation or vacuum centrifugation methods. Approximately 93 % of CIP (20 mg/L) could be removed by Fe_3O_4-sep-vacuum within 20 min at initial pH 6.0. The kinetic and adsorption isotherms followed pseudo-second-order and Temkin models, respectively. The obtained maximum adsorption capacity (q_m) for CIP by Fe_3O_4-sep-vacuum was 18.4 mg/g at initial pH 6.0. The solution pH, temperature, coexisting divalent cations, and HA concentration were likely controled the adsorption processes of CIP on Fe_3O_4-sep-vacuum surface. The addition of NaF and urea significantly inhibited the adsorption of CIP, indicating that hydrogen bonds and hydroxyl groups on the Fe_3O_4-sep-vacuum surface played crucial roles in the adsorption process. Electrostatic interactions and hydrogen bonding played decisive roles in the adsorption process of CIP by Fe_3O_4-sep-vacuum. Ion exchange, surface complexation, hydrophobic interaction and van der Waals interactions between CIP and Fe_3O_4-sep-vacuum surface might also contribute to the adsorption process of CIP. The Fe_3O_4-sep-vacuum maintained excellent adsorption performance after 5 cycles, indicating it had high stability and reusability. Fe_3O_4-sep-vacuum also had high adsorption capacity to ofloxacin. This study indicated that the highly dispersed Fe_3O_4 nanoparticles modified sepiolite composite could be served as a promising adsorbent material to apply in remediation of antibiotics contaminated wastewater. Our findings could also provide new insights into the design and fabrication of other high activity nanoparticles modified sepiolite composites with enhanced performance in eliminating pollutants from wastewater.

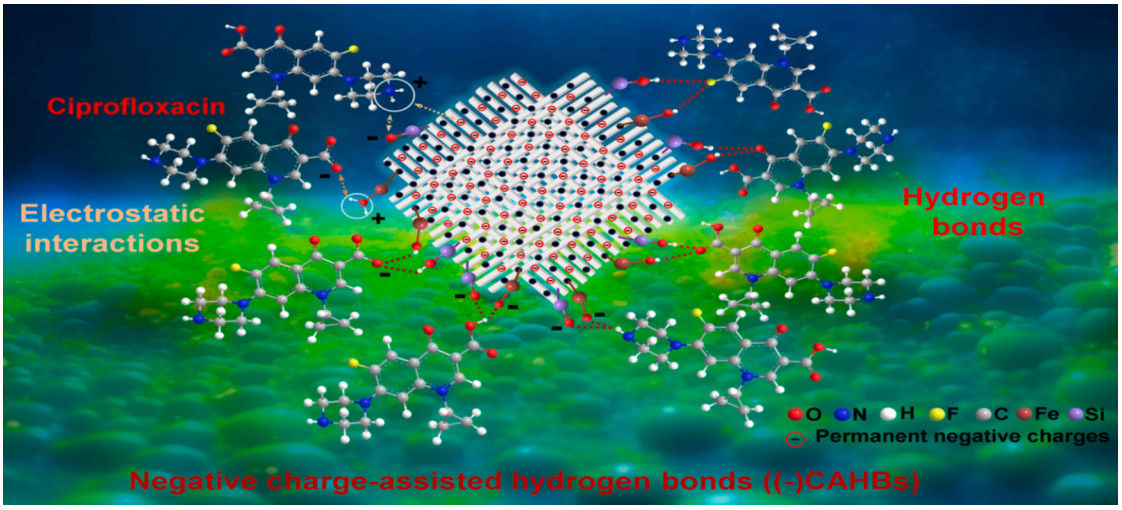

Fig. 8. Proposed mechanism for CIP adsorption by Fe_3O_4-sep-vacuum.

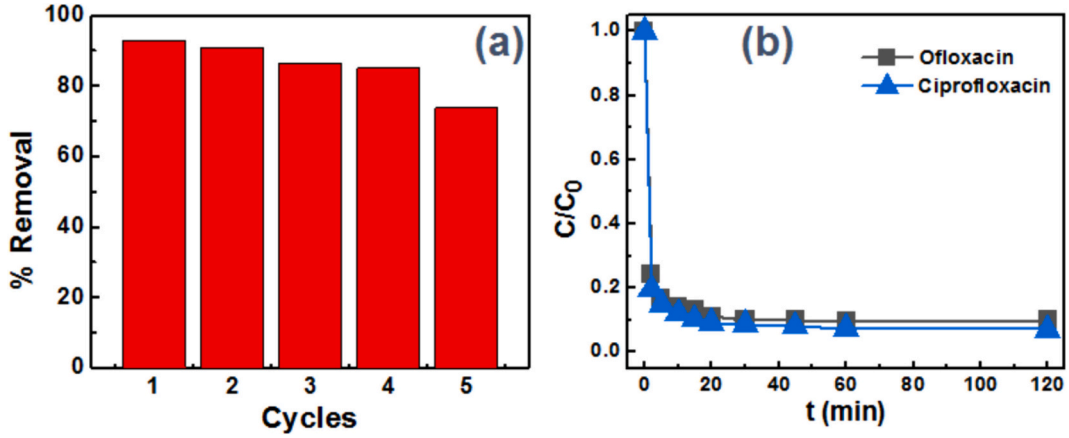

Fig. 9. (a) Stability and reusability of Fe_3O_4-sep-vacuum for removing CIP after 5 cycles; (b) The adsorption curves of 20 ppm CIP and ofloxacin by Fe_3O_4-sep-vacuum.

CRediT authorship contribution statement

Shiyuan Kang: Writing – original draft, Validation, Investigation, Data curation. **Bing Yi:** Writing – review & editing, Supervision. **Xin Nie:** Writing – review & editing, Validation, Supervision, Data curation, Conceptualization. **Quan Wan:** Supervision, Funding acquisition, Conceptualization. **Hai Yang:** Writing – review & editing, Supervision, Funding acquisition, Data curation, Conceptualization.

Declaration of competing interest

The authors declare that they have no known competing financial interests or personal relationships that could have appeared to influence the work reported in this paper.

Data availability

Data will be made available on request.

Acknowledgements

This work was financially supported by Hunan Natural Science Foundation for Distinguished Young Scholars (2021JJ10001), Guizhou Provincial Science and Technology projects ([2020]1Z039), National Natural Science Foundation of China (42377229, 41902041, 41872046), Huxiang High Level Talent Gathering Project (2021RC5011), and the Key Areas Research and Development Plan of Hunan Province (2021SK2038). The thanks also given to Dr. Weijie Zhang and Xiaomeng Yang for their help of data curation.

References

[1] A.C. Singer, H. Shaw, V. Rhodes, A. Hart, Review of antimicrobial resistance in the environment and its relevance to environmental regulators, Front. Microbiol. 7 (2016), https://doi.org/10.3389/Fmicb.2016.01728.
[2] G.Y. Li, H. Yang, T.C. An, Y.J. Lu, Antibiotics elimination and risk reduction at two drinking water treatment plants by using different conventional treatment techniques, Ecotoxicol. Environ. Saf. 158 (2018) 154–161, https://doi.org/10.1016/j.ecoenv.2018.04.019.
[3] X.G. Hu, Q.X. Zhou, Y. Luo, Occurrence and source analysis of typical veterinary antibiotics in manure, soil, vegetables and groundwater from organic vegetable bases, northern China, Environ. Pollut. 158 (2010) 2992–2998, https://doi.org/10.1016/j.envpol.2010.05.023.
[4] A.S. Oberoi, Y.Y. Jia, H.Q. Zhang, S.K. Khanal, H. Lu, Insights into the fate and removal of antibiotics in engineered biological treatment systems: a critical review, Environ. Sci. Technol. 53 (2019) 7234–7264, https://doi.org/10.1021/acs.est.9b01131.
[5] R. Hernández-Tenorio, E. González-Juárez, J.L. Guzmán-Mar, L. Hinojosa-Reyes, A. Hernández-Ramírez, Review of occurrence of pharmaceuticals worldwide for estimating concentration ranges in aquatic environments at the end of the last decade, Journal of Hazardous Materials Advances 8 (2022) 100172, https://doi.org/10.1016/j.hazadv.2022.100172.
[6] Q.Q. Zhang, G.G. Ying, C.G. Pan, Y.S. Liu, J.L. Zhao, Comprehensive evaluation of antibiotics emission and fate in the river basins of China: source analysis, multimedia modeling, and linkage to bacterial resistance, Environ. Sci. Technol. 49 (2015) 6772–6782, https://doi.org/10.1021/acs.est.5b00729.
[7] G.S. Zhang, W.Y. Li, S. Chen, W. Zhou, J.P. Chen, Problems of conventional disinfection and new sterilization methods for antibiotic resistance control, Chemosphere 254 (2020), https://doi.org/10.1016/j.chemosphere.2020.126831.
[8] X. Liu, J.C. Steele, X.Z. Meng, Usage, residue, and human health risk of antibiotics in Chinese aquaculture: a review, Environ. Pollut. 223 (2017) 161–169, https://doi.org/10.1016/j.envpol.2017.01.003.
[9] M. Qiao, G.G. Ying, A.C. Singer, Y.G. Zhu, Review of antibiotic resistance in China and its environment, Environ. Int. 110 (2018) 160–172, https://doi.org/10.1016/j.envint.2017.10.016.
[10] O.M. Rodriguez-Narvaez, J.M. Peralta-Hernandez, A. Goonetilleke, E.R. Bandala, Treatment technologies for emerging contaminants in water: a review, Chem. Eng. J. 323 (2017) 361–380, https://doi.org/10.1016/j.cej.2017.04.106.
[11] X. Nie, G. Li, S. Li, Y. Luo, W. Luo, Q. Wan, T. An, Highly efficient adsorption and catalytic degradation of ciprofloxacin by a novel heterogeneous Fenton catalyst of hexapod-like pyrite nanosheets mineral clusters, Appl Catal B 300 (2022) 120734, https://doi.org/10.1016/j.apcatb.2021.120734.
[12] W. Zhang, P. Sun, B. Wang, S. Li, B. Yi, Q. Liu, H. Yang, Polarization engineering of conjugated microporous polymers to boost exciton dissociation by dielectric constant regulation for photocatalytic degradation of antibiotics, Sep. Purif. Technol. 332 (2024) 125776, https://doi.org/10.1016/j.seppur.2023.125776.
[13] R.S. Monisha, R.L. Mani, B. Sivaprakash, N. Rajamohan, D.V.N. Vo, Green remediation of pharmaceutical wastes using biochar: a review, Environ. Chem. Lett. 20 (2022) 681–704, https://doi.org/10.1007/s10311-021-01348-y.
[14] L.M. Nguyen, N.T.T. Nguyen, T.T.T. Nguyen, T.T. Nguyen, D.T.C. Nguyen, T. V. Tran, Occurrence, toxicity and adsorptive removal of the chloramphenicol antibiotic in water: a review, Environ. Chem. Lett. 20 (2022) 1929–1963, https://doi.org/10.1007/s10311-022-01416-x.
[15] T. Paul, J.Y. Liu, M.L. Machesky, T.J. Strathmann, Adsorption of zwitterionic fluoroquinolone antibacterials to goethite: a charge distribution-multisite complexation model, J. Colloid Interface Sci. 428 (2014) 63–72, https://doi.org/10.1016/j.jcis.2014.04.034.
[16] M. Kah, G. Sigmund, F. Xiao, T. Hofmann, Sorption of ionizable and ionic organic compounds to biochar, activated carbon and other carbonaceous materials, Water Res. 124 (2017) 673–692, https://doi.org/10.1016/j.watres.2017.07.070.
[17] C.H. Li, F.L. Wang, X. Xu, Y.B. Shi, J.S. Liang, R.S. Yang, J. Liu, Z.L. Zhao, A high-capacity malleable cellulose aerogel with layered double hydroxide decorating ZIF-8 for efficient adsorption of ciprofloxacin, Chem. Eng. J. 455 (2023), https://doi.org/10.1016/j.cej.2022.140841.
[18] Z. Sayyar, Z. Hosseini, P.M. Pakdel, A. Hassani, Preparation of novel and low-cost chitosan modified with montmorillonite/ZnO hydrogel nanocomposite for adsorption of ciprofloxacin from water, J. Water Process Eng 63 (2024), https://doi.org/10.1016/j.jwpe.2024.105449.
[19] S. Rakshita, D. Sarkar, E.J. Elzinga, P. Punamiya, R. Datta, Mechanisms of ciprofloxacin removal by nano-sized magnetite, J. Hazard. Mater. 246 (2013) 221–226, https://doi.org/10.1016/j.jhazmat.2012.12.032.
[20] X.M. Xu, W.M. Chen, S.Y. Zong, X. Ren, D. Liu, Atrazine degradation using Fe_3O_4-sepiolite catalyzed persulfate: reactivity, mechanism and stability, J. Hazard. Mater. 377 (2019) 62–69, https://doi.org/10.1016/j.jhazmat.2019.05.029.
[21] B. Yi, J. Zeng, W.J. Zhang, H.S. Cui, H.J. Liu, C.T. Au, Q. Wan, H. Yang, Enhanced hydrophilicity and promoted charge transfer in covalent triazine frameworks/sepiolite complexed via hydrogen bonding for visible-light driven degradation of antibiotics, Appl. Clay Sci. 238 (2023), https://doi.org/10.1016/j.clay.2023.106921.

[22] F.F. Yang, A.Q. Wang, Recent researches on antimicrobial nanocomposite and hybrid materials based on sepiolite and palygorskite, Appl. Clay Sci. 219 (2022), https://doi.org/10.1016/j.clay.2022.106454.
[23] N. Zhang, N.X. Li, X.Y. Han, H. Zhang, J.P. Meng, P.F. Zhou, J.S. Liang, In-situ synthesis of sepiolite-supported ceria nanocrystal composites for efficient removal of aflatoxin B1: enhanced degradation of mycotoxins in the environment by sepiolite nanofibers, J. Alloys Compd. 960 (2023), https://doi.org/10.1016/j.jallcom.2023.170800.
[24] E. Eren, H. Gumus, N. Ozbay, Equilibrium and thermodynamic studies of Cu(II) removal by iron oxide modified sepiolite, Desalination 262 (2010) 43–49, https://doi.org/10.1016/j.desal.2010.05.039.
[25] E. Eren, H. Gumus, Characterization of the structural properties and Pb(II) adsorption behavior of iron oxide coated sepiolite, Desalination 273 (2011) 276–284, https://doi.org/10.1016/j.desal.2011.01.004.
[26] K. Hou, G.F. Wang, Y.P. Zhu, N. Ezzatahmadi, L.J. Fu, A.D. Tang, H.M. Yang, Y. F. Xi, Sepiolite/Fe_3O_4 composite for effective degradation of diuron, Appl. Clay Sci. 181 (2019), https://doi.org/10.1016/j.clay.2019.105243.
[27] A. Puente-Urbina, V. Montero-Campos, Porous materials modified with Fe_3O_4 nanoparticles for arsenic removal in drinking water, water, air, Soil Pollut. 228 (2017), https://doi.org/10.1007/s11270-017-3513-3.
[28] A.A. Ahribesh, S. Lazarevic, I. Jankovic-Castvan, B. Jokic, V. Spasojevic, T. Radetic, D. Janackovic, R. Petrovic, Influence of the synthesis parameters on the properties of the sepiolite-based magnetic adsorbents, Powder Technol. 305 (2017) 260–269, https://doi.org/10.1016/j.powtec.2016.09.086.
[29] A. Gürses, A. Hassani, M. Kıranşan, Ö. Açışlı, S. Karaca, Removal of methylene blue from aqueous solution using by untreated lignite as potential low-cost adsorbent: kinetic, thermodynamic and equilibrium approach, J. Water Process Eng 2 (2014) 10–21, https://doi.org/10.1016/j.jwpe.2014.03.002.
[30] Y. Yin, Y. Ren, J.H. Lu, W.M. Zhang, C. Shan, M. Hua, L. Lv, B.C. Pan, The nature and catalytic reactivity of UiO-66 supported Fe_3O_4 nanoparticles provide new insights into Fe-Zr dual active centers in Fenton-like reactions, Appl Catal B 286 (2021), https://doi.org/10.1016/j.apcatb.2021.119943.
[31] Q.J. Wang, A.D. Tang, L.F. Zhong, X. Wen, P. Yan, J.J. Wang, Amino-modified γ-Fe_2O_3/sepiolite composite with rod-like morphology for magnetic separation removal of Congo red dye from aqueous solution, Powder Technol. 339 (2018) 872–881, https://doi.org/10.1016/j.powtec.2018.08.055.
[32] N. Zhao, Q.Y. Ma, Y.F. Wei, S. Wang, X.M. Zhong, G.Z. Zhuang, P. Yuan, Co_3O_4 anchored on sepiolite surface grooves for superior adsorption of tetracycline from wastewater, Sep. Purif. Technol. 323 (2023), https://doi.org/10.1016/j.seppur.2023.124367.
[33] Q. Zhou, J.L. Huang, X. Zhang, Y. Gao, Assembling polypyrrole coated sepiolite fiber as efficient particle adsorbent for chromium (VI) removal with the feature of convenient recycling, Appl. Clay Sci. 166 (2018) 307–317, https://doi.org/10.1016/j.clay.2018.09.031.
[34] X.L. Xie, Y.L. Wang, M. Hao, P.J. Yan, J.S. Liang, D.X. Wang, H. Li, F. Wang, A WS_2/sepiolite composite with highly dispersed WS_2 nanosheets for photocatalytic wastewater treatment, Appl. Clay Sci. 228 (2022), https://doi.org/10.1016/j.clay.2022.106576.
[35] C.H. Liang, X.D. Zhang, P. Feng, H.X. Chai, Y.M. Huang, ZIF-67 derived hollow cobalt sulfide as superior adsorbent for effective adsorption removal of ciprofloxacin antibiotics, Chem. Eng. J. 344 (2018) 95–104, https://doi.org/10.1016/j.cej.2018.03.064.
[36] Q.L. Wu, X.F. Yang, J. Liu, X. Nie, Y.L. Huang, Y.P. Wen, J. Khan, W.U. Khan, M. M. Wu, T.C. An, Topotactic growth, selective adsorption, and adsorption-driven Photocatalysis of protonated layered Titanate Nanosheets, ACS Appl. Mater. Interfaces 6 (2014) 17730–17739, https://doi.org/10.1021/am5041847.
[37] S. Yadav, A. Asthana, A.K. Singh, R. Chakraborty, S.S. Vidya, M.A. Susan, S.A. C. Carabineiro, Adsorption of cationic dyes, drugs and metal from aqueous solutions using a polymer composite of magnetic/β-cyclodextrin/activated charcoal/Na alginate: isotherm, kinetics and regeneration studies, J. Hazard. Mater. 409 (2021), https://doi.org/10.1016/j.jhazmat.2020.124840.
[38] Y.W. Zhu, Q.X. Yang, T.T. Lu, W. Qi, H.J. Zhang, M.J. Wang, Z.C. Qi, W.F. Chen, Effect of phosphate on the adsorption of antibiotics onto iron oxide minerals: comparison between tetracycline and ciprofloxacin, Ecotoxicol. Environ. Saf. 205 (2020), https://doi.org/10.1016/j.ecoenv.2020.111345.
[39] X. Nie, Q. Wan, M.F. Hochella, S.X. Luo, M.Z. Yang, S.S. Li, Y.H. Fu, P. Zeng, Z. H. Qin, W.B. Yu, Interfacial adsorption of gold nanoparticles on arsenian pyrite: new insights for the transport and deposition of gold nanoparticles, Chem. Geol. 640 (2023), https://doi.org/10.1016/j.chemgeo.2023.121747.
[40] R.Y. Xie, X.H. Xing, X. Nie, X.S. Ma, Q. Wan, Q.S. Chen, Z.X. Li, J.X. Wang, Deposition behaviors of carboxyl-modified polystyrene nanoplastics with goethite in aquatic environment: effects of solution chemistry and organic macromolecules, Sci. Total Environ. 904 (2023), https://doi.org/10.1016/j.scitotenv.2023.166783.
[41] W. Wang, J.D. Cheng, J. Jin, Q. Zhou, Y. Ma, Q.Q. Zhao, A.M. Li, Effect of humic acid on ciprofloxacin removal by magnetic multifunctional resins, Sci. Rep. 6 (2016), https://doi.org/10.1038/srep30331.
[42] Y.Q. Wu, Y.Q. Shi, H.L. Wang, Urea as a hydrogen bond producer for fabricating mechanically very strong hydrogels, Macromolecules (2023), https://doi.org/10.1021/acs.macromol.3c00611.
[43] M. Zandieh, J.W. Liu, Removal and degradation of microplastics using the magnetic and Nanozyme activities of bare Iron oxide nanoaggregates, Angew. Chem. Int. Ed. 61 (2022), https://doi.org/10.1002/anie.202212013.
[44] Y.P. Bao, N.S. Bolan, J.H. Lai, Y.S. Wang, X.H. Jin, M.B. Kirkham, X.L. Wu, Z. Fang, Y. Zhang, H.L. Wang, Interactions between organic matter and Fe (hydr)oxides and their influences on immobilization and remobilization of metal(loid)s: a review, Crit. Rev. Environ. Sci. Technol. 9 (2021) 1–22, https://doi.org/10.1080/10643389.2021.1974766.
[45] C.A. Igwegbe, S.N. Oba, C.O. Aniagor, A.G. Adeniyi, J.O. Ighalo, Adsorption of ciprofloxacin from water: a comprehensive review, J. Ind. Eng. Chem. 93 (2021) 57–77, https://doi.org/10.1016/j.jiec.2020.09.023.